JOURNAL OF CATALYSIS **173,** 333–344 (1998)
ARTICLE NO. CA971905

Structural and Textural Characterization of $AlPO_4$–B_2O_3 and Al_2O_3–B_2O_3 (5–30 wt% B_2O_3) Systems Obtained by Boric Acid Impregnation

Felipa M. Bautista,* Juan M. Campelo,*,[1] Angel Garcia,* Diego Luna,* Jose M. Marinas,* Maria C. Moreno,* Antonio A. Romero,* Jose A. Navio,† and Manuel Macias†

*Departamento Química Orgánica, Universidad de Córdoba, Avda. San Alberto Magno, s/n°, E-14004 Córdoba, España; and †Instituto de Ciencias de Materiales de Sevilla, Centro de Investigaciones Científicas "Isla de la Cartuja," Avda. Américo Vespucio, s/n°, E-41092 Sevilla, España

Received May 19, 1997; revised September 17, 1997; accepted September 22, 1997

A series of $AlPO_4$–B_2O_3 (APB) and Al_2O_3–B_2O_3 (AlB) systems with various boria loadings (5–30 wt%) were prepared by impregnation of $AlPO_4$ with boria from a boric acid solution (methanol or water) and characterized by XRD, SEM-EDX, TG/DTA, XPS, DRIFT and nitrogen adsorption. ^{11}B, ^{27}Al, and ^{31}P MAS NMR were used to determine the local structure. DTA and XRD analysis showed that crystallization occurred in all cases above 900 K, yielding α-cristobalite-$AlPO_4$ in APB systems, and aluminum borate in AlB systems. Also, boron oxide remained amorphous (XRD) for thermal treatments in the range 473–1073 K. SEM showed a non-homogeneous distribution in morphology, texture and particle size. Also, EDX and XPS indicated a surface enrichment in boron for APB systems while for AlB ones the reverse is true. Moreover, ^{27}Al MAS NMR showed the simultaneous presence of four and six-coordinate Al atoms in AlB systems while in APB ones, Al atoms appeared only in $Al(OP)_4$ environments. ^{31}P MAS NMR only identified P atoms with tertrahedral coordination. Besides, the presence of boria did not change the local structure of the starting $AlPO_4$ or Al_2O_3 support. ^{11}B MAS NMR identified both tetrahedral (BO_4) and trigonal (BO_3) species as being present; the concentration of tetrahedral oxygen coordinated borate (BO_4) species were found to increase with boria loading. Furthermore, DRIFT spectroscopy showed that the incorporation of boron results in the appearance of B–OH groups and B–O stretches of a borate phase where both trigonal and tetrahedral boron exist on the surface of APB and AlB samples. Besides, trigonal borate species predominate and tetrahedral borate species increase with boron loading. Finally, the incorporation of boron produces a decrease in surface area and pore volume that becomes greater as the boron content increases.

INTRODUCTION

$AlPO_4$ can be used as a catalyst and support. As a catalyst, $AlPO_4$ is known to be active in several chemical processes, such as dehydration, isomerization, alkylation, rearrangement, retroaldolization, condensation, and Diels-Alder cycloaddition (1–15). Moreover, $AlPO_4$ is also used as a support for polymerization, oxidation, hydrogenation, reductive cleavage or hydration catalysts (1, 16–24). The acid-base properties of $AlPO_4$ play an important role in catalytic reactions. By modifying the acid-base properties of $AlPO_4$, the catalytic activity can be controlled. Modification of an aluminum starting salt (2), calcination at high temperatures (1, 2, 13), the addition of alkali (3), fluoride (4) and sulfate (5) ions and a metal oxide (1, 10–20) bring about changes in the physico-chemical properties and catalytic activities of $AlPO_4$. In the latter case, the performance of such catalysts is greatly dependent on the nature of the metal oxide (Al_2O_3, SiO_2, TiO_2, ZrO_2, ZnO, V_2O_5, MoO_3 or WO_3), the $AlPO_4$/metal oxide ratios, the methods of preparation and operating conditions (1, 10–20).

Moreover, the incorporation of boron oxide to Al_2O_3 leads to an alumina-boria catalyst with an increase in the acid character in relation to pure Al_2O_3. Acid behaviors are reported to be due to Brønsted acid sites (25, 26) so that surface acidities and, hence, catalytic activities are found to change with boria loading. Increased acidity is reflected in their ability to perform acid-catalyzed conversions and thus alumina-boria were found to be active catalysts in several vapor-phase reactions such as toluene disproportionation (25, 26), m-xylene (25, 26) and 1-butene (27) isomerization, Beckmann rearrangement of cyclohexanone oxime (26, 28–30), n-octane hydroconversion (31) and 2-propanol (32–34) and methanol (35) dehydration, and ethane partial oxidation (36). Also, Al_2O_3–B_2O_3 systems have been used as the support for Co–Mo and Ni–Mo hydrotreating catalysts (37, 38).

Alumina-boria catalysts are readily prepared by impregnation methods, using boric acid solution and an alumina support (25, 27, 34, 39, 40) or by coprecipitation from aluminum nitrate and boric acid, using an ammonium hydroxide solution (31–34). More recently, alumina-boria catalysts have been prepared by low-temperature thermal decomposition of aluminum nitrate and boric acid sustained by the simultaneous oxidation of a suitable organic agent like

[1] To whom correspondence should be addressed.

0021-9517/98 $25.00

glycerol (35, 41). The activity of the alumina-boria catalyst was considerably affected by the chemical and the physical nature of the alumina used as the catalyst base as well as by the conditions of catalyst preparation.

In order to gain more insight into the possibilities of using $AlPO_4$ as a support for metal oxides in acid-base catalysis, in the present work a series of $AlPO_4$–B_2O_3 systems, with various amounts of B_2O_3, have been prepared by impregnation of $AlPO_4$ with boric acid solution (methanol or water). For comparison, a series of Al_2O_3–B_2O_3 (5–30 wt% B_2O_3) were also prepared by boric acid impregnation of a home made γ-Al_2O_3. The resulting solids have been characterized by TG and DTA measurements, X-ray diffraction (XRD), X-ray photoelectron spectroscopy (XPS), scanning electron microscopy coupled with energy-dispersive X-ray analysis (SEM-EDX), diffuse reflectance infrared spectroscopy (DRIFT), high resolution ^{11}B, ^{27}Al, and ^{31}P MAS NMR and nitrogen adsorption.

The studies of surface acidity and catalytic activity of $AlPO_4$–B_2O_3 and Al_2O_3–B_2O_3 systems are now in progress. Thus, initial results in cyclohexene skeletal isomerization show that Al_2O_3–B_2O_3 catalysts are more active than $AlPO_4$–B_2O_3 ones. These results can be well interpreted in terms of the acidic characteristics of catalysts. Moreover, $AlPO_4$–B_2O_3 catalysts are more active and selective than AlB ones for the Beckmann rearrangement of cyclohexanone oxime to ε-caprolactam, commercially important product in the manufacture of synthetic fibers (specially nylon 6) and in many other applications.

EXPERIMENTAL

Catalysts

$AlPO_4$ support (AP-773) was obtained from aluminum chloride and orthophosphoric acid by precipitation with aqueous ammonia until the pH of the supernatant was 7. The precipitate was allowed to stand at room temperature for 18 h; the final pH after this time was 6.1. After filtration, it was washed several times with propan-2-ol. Afterwards, the gel was dried at 393 K for 24 h and calcined at 773 K for 3 h.

Al_2O_3 support (Al-923) was obtained from aluminum nitrate by precipitation with aqueous ammonia until the pH of the supernatant was 7. The precipitate was allowed to stand at room temperature for 18 h. After filtration, it was washed several times with propan-2-ol. Afterwards, the gel was dried at 393 K for 24 h and calcined at 923 K for 3 h.

$AlPO_4$–B_2O_3 (APB) and Al_2O_3–B_2O_3 (AlB) systems, with different boria loadings (5–30 wt%), were prepared by incipient wetness impregnation using an aqueous or a methanolic solution of boric acid. After soaking the system in this solution for 1 h, the impregnated supports were dried at 393 K for 24 h and then calcined at 473, 573, and 623 K for 3 h. The $AlPO_4$–B_2O_3 and Al_2O_3–B_2O_3 systems are designated by APB and AlB, respectively, followed by two numbers, hyphen separated, that indicate respectively, the boria loading and the calcination temperature (APB-9-473, AlB-9-623, etc.). When the systems were prepared from a methanolic boric acid solution, the letter M is included between the two numbers (APB-9-M-573, AlB-20-M-573, and so on).

Unmodified $AlPO_4$ was prepared by placing it in water or methanol (M) containing no boric acid, drying at 393 K for 24 h, and later on calcining at 473, 573, and 623 K for 3 h. Unmodified Al_2O_3 were prepared similarly. These samples are designated by AP-0 (or AP-0-M) and Al-0 (or Al-0-M) followed by the calcination temperature.

Diboron trioxide (B_2O_3) was prepared by calcination of boric acid at 473–1073 K for 3 h. The samples are designated by B followed by the calcination temperature (B-473, B-573, etc.).

Thermogravimetry and Differential Thermal Analysis

Thermogravimetric (TG) and differential thermal analyses (DTA) were obtained simultaneously using a high-temperature thermal analyzer Setaram 92, model 16.18, in the presence of static air at a heating rate of 10 K min^{-1} (temperature range: 273–1473 K). Finely powdered α-alumina was used as a reference material. The samples used were the dried boric acid impregnated supports (393 K, 24 h) prior to calcination.

X-Ray Diffraction Measurements

X-ray studies of the thermal products were carried out using a Siemens D-500 diffractometer fitted with an automatic control and data acquisition system (DACO-MP). The patterns were run with nickel-filtered copper Kα radiation ($\lambda = 1.5405$ Å) at 35 KV and 20 mA; the 2θ diffraction angle (5–75°) was scanned at a rate of $2°(2\theta)$ min^{-1}.

Scanning Electron Microscopy (SEM)

SEM studies were carried out in a Jeol apparatus, model JSM-5400, and the dispersion energy of X-rays (EDX) was measured by a Link Isis Pentafet Model analyzer; a semiautomatic image analyzer of magnetostrictive KONTRON MOP-30 board was used to estimate the average weight size of aggregates and particles.

XPS Measurements

The XPS spectra were recorded on a Leybold-Heraeus LHS-10 spectrometer working with a pass energy constant of 50 eV and using Al Kα radiation ($h\nu = 1686.6$ eV) as the excitation source. The spectra were submitted to background substraction and to area calculations. Binding energy values were referenced to the C(1s) peak (pollution carbon) at 284.6 eV.

NMR Spectroscopy

^{11}B (pulse: 0.4 μs; recycle delay: 2 s), ^{27}Al (pulse: 0.6 μs; recycle delay: 0.3 s) and ^{31}P (pulse: 2.6 μs; recycle delay: 6 s) MAS NMR spectra were recorded at resonance frequencies ν_0 of 128.38, 104.26, and 128.38 MHz, respectively, with a Bruker ACP-400 multinuclear spectrometer (external magnetic field of 9.4 T). ^{1}H–^{11}B CP MAS spectra were acquired with a single-contact-time pulse sequence, 4.8 μs ^{1}H $\pi/2$ pulses, and 2 s recycle delays.

NMR measurements were carried out on samples previously dried at 413 K for at least 96 h. Immediately after that had been dried, the samples were rapidly transferred to spinners in order to keep hydration effects to a minimum. Measurements were carried out at room temperature with a standard Bruker double-bearing MAS (5.6 kHz) probe. About 200 mg of sample material was placed in the zirconium dioxide rotor (4 mm) with a volume of about 0.35 cm^3.

^{11}B MAS NMR were also recorded at a resonance frequency ν_0 of 160.46 MHz (pulse: 1 μs; recycle delay: 1 s) with a Bruker DSX-500 spectrometer operating at 11.7 T [Bruker, Wisemburg (France)]. In this case, rapid rotation at rates as high as 18 kHz was achieved with a high-speed MAS probehead (Bruker). The rotors have a diameter of 4 mm. Up to 7800 scans at 18 kHz were carried out in order to attain the real bandwidth of the spectra.

In order to preserve quantitative analysis, no mathematical procedures of NMR signal treatment, such as multiplication by an exponential function, were used. Also, the chemical shifts given for aluminum and boron were not corrected for second-order quadrupole effects. The references for ^{11}B, ^{27}Al and ^{31}P were external $BF_3 \cdot Et_2O$, $Al(H_2O)_6^{3+}$ and 85% H_3PO_4, respectively.

DRIFT Measurements

DRIFT spectra were recorded on an FTIR instrument (Bomen MB-100) equipped with an 'environmental chamber' (Spectra Tech, P/N 0030-100) placed in a diffuse reflectance attachment (Spectra Tech, Collector). A resolution of 8 cm^{-1} was used with 256 scans averaged to obtain a spectrum from 4000 to 400 cm^{-1}. Single-beam spectra were ratioed against KBr or support reference spectra collected at the same temperature as the sample. In the latter mode of presentation, the downward bands are due to decreased species (in the progress of the boria loading) and the upward bands are attributable to the species formed. A plot of pseudo-absorbance was preferred. This allowed direct subtraction of spectra obtained with the same sample under different conditions. The temperature controller was calibrated to the actual temperature by inserting a thermocouple directly into the sample and monitoring the sample temperature at different controller settings. The samples were diluted to 15% in KBr.

DRIFT spectra have been recorded for all the calcined catalysts previously dried at 400 K for 24 h under vacuum. Afterwards, the catalyst was placed in the environmental chamber cell with a 20 cm^3 min^{-1} flow of dehydrated and deoxygenated nitrogen, heated to 573 K and held at this temperature for 1 h prior to carrying out the spectrum. Longer nitrogen flushing times or vacuum treatment do not modify the DRIFT spectra. In some cases, spectra of the O–H stretching region were smoothed with a five-point Savitzky-Golay algorithm.

Surface Area and Pore Properties

Surface-area and pore-size information were obtained from nitrogen adsorption-desorption isotherms at 77 K, using a Micromeritics ASAP 2000 analyzer. Prior to measurements, all samples were degassed to 0.1 Pa. BET surface areas were calculated assuming a cross-sectional area of 0.162 nm^2 for the nitrogen molecule. Assessments of possible microporosity were made from *t*-plot constructions, using the Harkins-Jura correlation for t as a function of p/p_0. Parameters were fitted to a low-area, non-porous silica. Mesopore size distributions were calculated using the Barret-Joyner-Halenda (BJH) method, assuming a cylindrical pore model (42).

RESULTS AND DISCUSSION

TG/DTA Measurements

The weight-temperature and DTA profiles for the APB-9, APB-9-M and APB-30-M are shown in Fig. 1. The remaining APB samples display almost the same behavior. The TG profiles are characterized by a weight loss up to 563 K. Below 563 K the weight loss, accompanied by an endothermic band at 399 K in the DTA profile, can be attributed to the desorption of physically adsorbed methanol and/or water. Between 563 and 1473 K, a slight weight loss in observed, due mainly to the condensation of surface hydroxyls, together with an exothermic DTA peak (without a corresponding DTG peak). Thus, we can therefore establish that the exothermic transition corresponds to a crystallization of the amorphous mass (see XRD results below). The position of this band depends on the impregnation medium and boria loading of the APB system. For systems obtained from boric acid methanol solutions and boria loadings up to 9 wt%, the exothermic peak remained at around 1295 K, the same as for the pure AP support (not shown). However, as boria loading increased, the exothermic peak shifted to lower temperatures and thus, for a 30 wt% B_2O_3, it appeared at 1103 K.

Furthermore, for APB systems obtained from aqueous boric acid solution, the position of the exothermic peak shifted to lower temperatures in relation to the respective APB systems prepared in methanol: 1298 and 1002 K for APB-9-M and APB-9, respectively. So, crystallization of

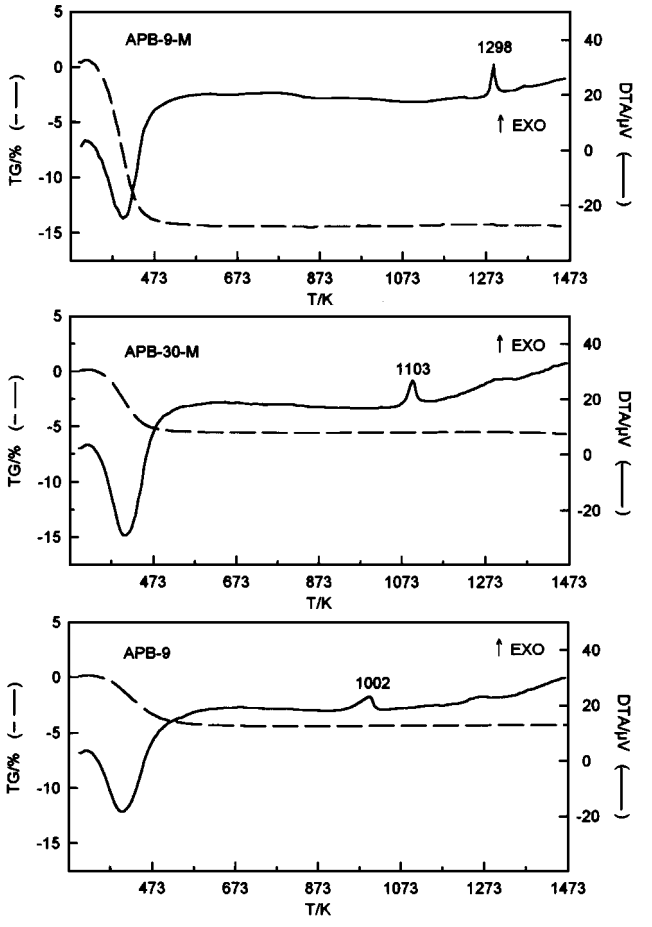

FIG. 1. TG and DTA curves for APB-9-M, APB-30-M and APB-9 samples. Static air atmosphere; 10 K min^{-1} scan.

the APB system is delayed when using methanol as impregnation solvent. Moreover, the small exothermic peak at around 1250 K could be assigned to the transformation of tridymite-$AlPO_4$ into α-cristobalite-$AlPO_4$ (see below).

As regards Al_2O_3–B_2O_3 systems (results not shown), the TG profiles are characterized by a weight loss up to 773 K, that was accompanied by an endothermic band at 379 K in the DTA, due to desorption of adsorbed methanol and/or water. From 773 K, a slight weight loss due to condensation of surface hydroxyls is found. In addition, DTA shows a broad exothermic peak whose position, as in APB systems, depends on the impregnation medium and boria loading (from 1368 K for AlB-9-M to 1175 K for AlB-30-M). XRD results (see below) indicated that this exothermic transition corresponds to the crystallization of an aluminum borate.

XRD Measurements

APB samples. From XRD analysis it was found that, in all APB systems and for calcination temperatures up to 623 K, only a very broad band was obtained in the range 15–26° (2θ). No other reflections could be found, indicating the amorphous nature of the $AlPO_4$ support and the boron oxide in APB systems regardless of boria loading (Fig. 2a).

After DTA measurements (thermal treatment at 1473 K), the $AlPO_4$ showed sharp diffraction lines (Fig. 2b–d) indicating the development of crystalline phases: a mixture of tridymite and α-cristobalite (Fig. 2b and 2c), which is enriched in the α-cristobalite phase (orthorhombic symmetry; ASTM index: 11–500) as boria loading increases (Fig. 2d). Aluminum borate diffraction peaks were not observed.

Moreover, Fig. 2a also showed that immediately before the DTA exotherm, the APB system remained amorphous. Thus, we can therefore establish that exothermic transition corresponds to a crystallization of the amorphous mass to crystallized $AlPO_4$.

AlB samples. From XRD analysis it was found that, for all AlB systems and temperature treatments below the DTA exothermic peak (Fig. 3a), broad diffraction patterns are observed. These patterns corresponds to a γ-Al_2O_3 [$2\theta = 37°$ (d = 2.43 Å); $2\theta = 46°$ (d = 1.79 Å); $2\theta = 67°$ (d = 1.40 Å); ASTM index: 10–425] with a low order of crystallinity.

As in APB systems, the characteristic bands of crystalline boron oxide (ASTM index: 6–297) did not appear which indicated the amorphous nature of boria in AlB systems regardless of their loading.

Moreover, after DTA measurements (thermal treatments at 1473 K), the AlB systems showed sharp X-ray diffraction patterns (Fig. 3b) characteristics of the formation of an $9Al_2O_3 \cdot 2B_2O_3$ aluminum borate [$2\theta = 16.5$ (d = 5.37 Å); $2\theta = 20.3$ (d = 4.36 Å); $2\theta = 26.4$ (d = 3.373 Å);

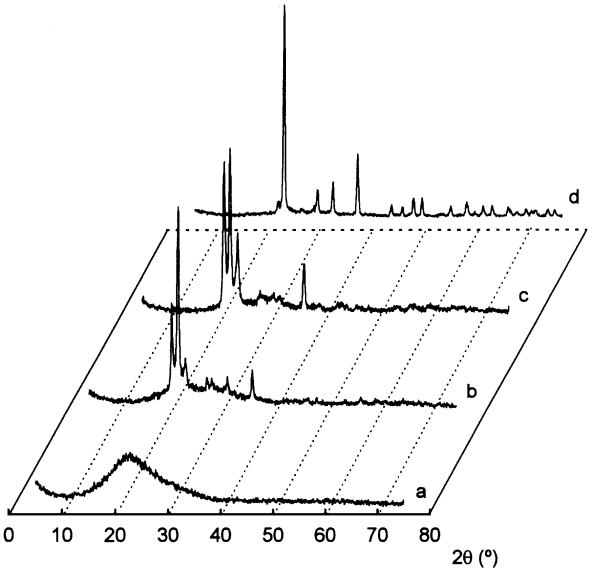

FIG. 2. XRD patterns (Cu-K_α radiation). (a) $AlPO_4$ and APB systems treated at temperatures up to 1250 K, (b) AP-1473, (c) APB-9-M-1473, and (d) APB-30-M-1473.

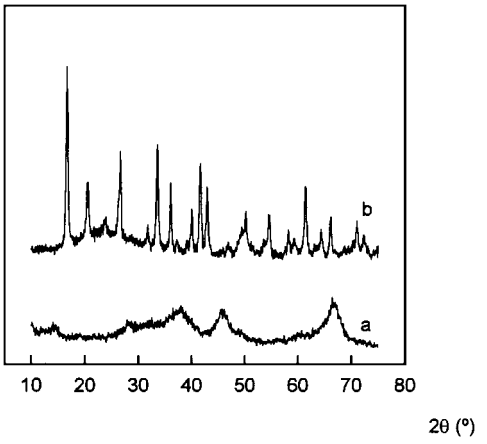

FIG. 3. XRD patterns (Cu-K_α radiation). (a) Al_2O_3 and AlB systems treated at temperatures up to 1250 K and (b) AlB-30-M-1473.

$2\theta = 33.3$ (d = 2.685 Å); $2\theta = 35.8$ (d = 2.505 Å); $2\theta = 41.3$ (d = 2.181 Å); $2\theta = 42.7$ (d = 2.116 Å); $2\theta = 61.2$ (d = 1,513 Å); ASTM index: 32–3]. The intensity of these bands increased with boria loading. At low boria loading, bands corresponding to α-Al_2O_3 (ASTM index: 10–173) also appeared although with low intensity. In the absence of boron oxide, the γ-Al_2O_3 was converted to α-Al_2O_3 at 1273 K (1).

As regards the Al_2O_3–B_2O_3 system, three crystalline forms have been discovered: two orthorhombic phases, $9Al_2O_3 \cdot 2B_2O_3$ (denoted as A_9B_2) and $2Al_2O_3 \cdot B_2O_3$ (denoted as A_2B), and a hexagonal phase $AlBO_3$ (43). The orthorhombic phases can be prepared by heating a mixture of Al_2O_3 and B_2O_3. Above 1308 K, only the A_9B_2 phase is thermodynamically stable (44): This structure has been characterized by XRD (45). It consists of infinite octahedral chains of edge-sharing AlO_6 octahedral running parallel to the crystallographic c axis. These chains are interlinked by two different types of five-fold coordinated AlO_5 polyhedra and by AlO_4 tetrahedra. The BO_3 groups occur as planar arrangements in parallel sheets (010). In this structure, there are open channels which run parallel to the c axis.

Boria samples. XRD analysis showed that boron oxide obtained from boric acid calcination at temperatures in the range 473–1073 K, remained amorphous (results not shown). In this sense, boria is known to be one of the most difficult substances to crystallize, and in its vitreous state the structure consists of a 3-D network of partially ordered trigonal BO_3 units. The network consists of two different structural units: the boroxol ring (in which three borons are linked by three oxygens to form a six-membered ring structure and all the borons are three-coordinated and constrained to be planar by delocalized π-bonding) and non-ring BO_3 units. Both units are linked together through bridging oxygens (46, 47).

SEM and XPS Studies

SEM micrographs of APB-30-M and AlB-30-M systems calcined at 573 (3 h) are shown in Fig. 4.

In APB systems SEM micrographs (Fig. 4a) showed a very non-homogeneous distribution in morphology, texture and particle sizes. The average size of the particles was around 40 μm. Besides, great differences in samples obtained by impregnation in water or/in methanol do not appear. Moreover, EDX (results not shown) and XPS (Table 1) indicated a surface enrichment in boron, but, the surface composition of different particles types remained almost unchanged (EDX).

On the other hand, as can be seen from table 1, the surface concentration ratio $[P]_s/[Al]_s$ of APB systems is practically the same as the unmodified one (P/Al = 1). Besides, the various core lines investigated for different samples were very similar and all appeared as single symmetrical lines, indicating a homogeneous distribution of the electron densities around the atoms throughout the solid. Table 1 also lists the XPS binding energies (eV) of elements present on the

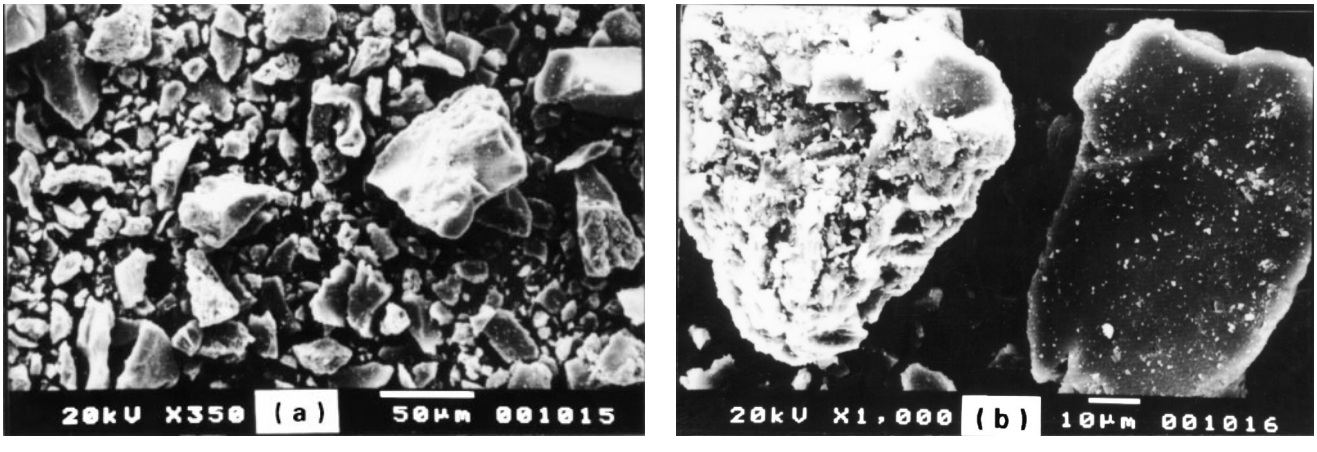

FIG. 4. SEM micrographs: (a) APB-30-M-573; (b) AlB-30-M-573.

TABLE 1

Elemental Surface Composition and XPS Binding Energies[a] of the Elements Present on the Surface and Elemental Bulk Composition of APB and AlB Systems Calcined at 573 K for 3 h

	Surface concentration (at%)					
	XPS			Stoichiometric values		
System	P (2p)	Al (2p)	B (1s)	P	Al	B
APB-9-M-573	11.1 (135.3)	11.8 (75.8)	29.7 (192.6)	14.5	14.5	5.1
APB-30-M-573	9.7 (135.7)	10.3 (76.3)	31.1 (193.3)	10.2	10.2	15.4
AlB-9-M-573	—	33.7 (74.2)	3.9 (192.1)	—	34.8	5.1
AlB-30-M-573	—	26.9 (75.1)	11.8 (193.2)	—	24.6	15.4

[a] In parenthesis, eV.

surface of samples. All values were referenced to the C (1s) peak at 284.6 eV. The increase in boron binding energy with boria loading could be due to the increase in BO_4/BO_3 ratio.

AlB systems also exhibited a very widely varied distribution in morphology, texture and particle sizes. The average size of the particles was around 30–35 μm. In these systems, EDX (results not shown) and XPS (Table 1) showed a decrease in superficial boron compared to stoichiometric values. Besides, superficial boron distribution depends on the preparation method and, thus, results are more homogeneous when using methanol as solvent. Furthermore, superficial boron amount and homogeneity increases as boria loading increases and, thus, for AlB-30-M-573 (Fig. 4b) there are no changes in the surface compositions of different particles (EDX).

NMR Spectroscopy

^{27}Al and ^{31}P MAS NMR spectroscopy. ^{27}Al and ^{31}P MAS NMR spectra of $AlPO_4$ support and Al_2O_3 calcined at 923 K (γ-Al_2O_3) and 1273 K (α-Al_2O_3) have been reported elsewhere (48). Thus, the positions of the tetrahedral component of $AlPO_4$ do not correspond to that of the γ-Al_2O_3 phase, showing that aluminum atoms occupy different environments in each type of sample. Also, during thermal treatment of $AlPO_4$ up to 1273 K, aluminum is not segregated as Al_2O_3 (48). Similar results concerning Al and P arrangements in amorphous compounds, obtained during coprecipitation of aluminophosphate catalysts with different P/Al ratios, have been reported by Cheung *et al.* (49).

APB samples. The ^{27}Al MAS NMR spectra (Fig. 5) showed the presence of a broad peak at around 37 ppm, typical of tetrahedral aluminum with phosphorus in the second coordination sphere, i.e. sharing oxygens with four tetrahedral of phosphorus [$Al(OP)_4$] (50, 51). The strong upfield shift observed with respect to other aluminum oxides is attributed by Muller *et al.* (50) to the influence of P atoms located in the second coordination sphere of Al. Moreover, the ^{31}P MAS spectra (Fig. 5) also showed one single broad component whose isotropic chemical shift value appeared at around −27 ppm. This chemical shift corresponded to P atoms in tetrahedral coordination with P−O−Al bonds [i.e., $P(OAl)_4$ environments]. Besides, it appears that the chemical shifts of P at different sites are similar, resulting in a broadened peak. Furthermore, the incorporation of boria did not change the isotropic chemical shift value of the ^{27}Al and ^{31}P peaks so that the local structure of the $AlPO_4$ support did not change by

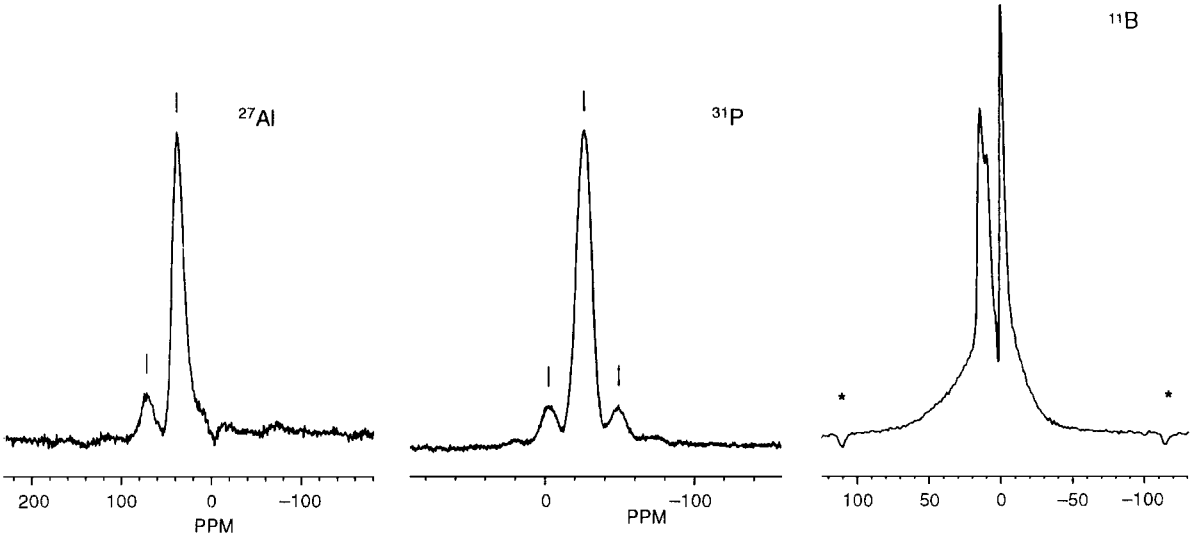

FIG. 5. ^{27}Al (9.4 T; 5.6 kHz MAS), ^{31}P (9.4 T; 4 kHz MAS) and ^{11}B (11.7 T; 18.1 kHz MAS) NMR spectra of APB-30-M-573 system.

boria; the spectra of APB samples was very similar to those obtained for AP-0 and AP-0-M samples.

AlB samples. The ^{27}Al MAS spectra (not shown) indicated the presence of two signals with different intensities, at approximately +39 and 9 ppm, unanimously accepted to originate from four and six-coordinate Al atoms, respectively (52, 53); their relative intensities were almost unchanged for samples with different boron contents and heating temperatures in the range 473–623 K. The relative AlO_6 : AlO_4 integrated intensities are nearly 3.1 : 1.0, which approximate the model of γ-Al_2O_3 as a defect spinel (54).

The incorporation of boria, therefore, did not change the local structure of the starting Al_2O_3 support when calcining in the range 473–623 K.

^{11}B MAS NMR spectroscopy. In glasses (55, 56), silicates (56, 57) and zeolites (57, 58) as well as in amorphous and crystalline borate compounds (27, 56, 59, 60) boron may exist in tetrahedral BO_4 units and trigonal BO_3 units. ^{11}B has spin I = 3/2 and thus an electric quadrupole moment. Tetrahedral BO_4 and trigonal BO_3 units have similar isotropic chemical shifts but substantially different quadrupolar coupling constants. Under MAS at high magnetic fields, the ^{11}B NMR spectra of tetrahedral BO_4 usually gives a relatively narrow single sharp signal in the range −5 to 2 ppm from boron trifluoride etherate ($BF_3 \cdot EtO_2$), indicating a highly symmetrical arrangement of the four oxygens in the BO_4 tetrahedron in the framework. Moreover, trigonal boron (BO_3) produces a characteristic quadrupolar doublet pattern in the range 19–12 ppm due to its high quadrupolar interaction. ^{11}B–^{1}H dipole interaction is removed by an intense proton decoupling, and ^{11}B–^{11}B and ^{11}B–^{10}B interactions are slight when a large distance exists between boron atoms. However, the ^{11}B chemical shift range is small and the peaks corresponding to the two boron coordinations often cannot be clearly separated. Turner *et al.* (56) indicate that rapid sample spinning (≥6 kHz) together with high-power proton decoupling, is generally desirable for rapid acquisition of ^{11}B NMR spectra of borates and borosilicates, from which accurate trigonal/tetrahedral ratios may be determined.

Figure 6 shows a series of ^{11}B MAS spectra (at 9.4 T) of various crystalline model compounds and the characteristic signals arising from trigonal and tetrahedral boron. Thus, crystalline boron phosphate (BPO_4, Fig. 6a) has all of the ^{11}B tetrahedrally coordinated with oxygen. Because of this tetrahedral coordination, the ^{11}B is in a highly symmetrical environment and its corresponding NMR signal is very sharp, appearing at −4.5 ppm from $BF_3 \cdot Et_2O$. Boron oxide (Fig. 6b), on the other hand, has all of its ^{11}B trigonally coordinated with oxygen (in six-membered boroxol rings and non-ring BO_3 units) and due to the fact that boron is a quadrupolar nucleus, quadrupolar splitting of the BO_3 signal occurs resulting in a broadened signal which resembles a doublet. Furthermore, the field strength used here resulted in an overlap of the trigonal and tetrahedral signals as shown in Figs. 6c and 6d where lithium tetraborate ($Li_2B_4O_7$) and borax ($Na_2B_4O_7 \cdot 10H_2O$) appeared, respectively. The structure of sodium and lithium tetraborates is based on two non-equivalent types of boron environments (61), a fact that is readily apparent from the 11.7 T spectra (not shown) but not in the 9.4 T spectra (Fig. 6) where the lower frequency feature of the doublet is embedded in the peak at the higher field which is due to boron with tetrahedral local symmetry. Thus, summarizing, the low field doublet arises from BO_3 units, while the sharp, high field line arises from the tetrahedral BO_4 units.

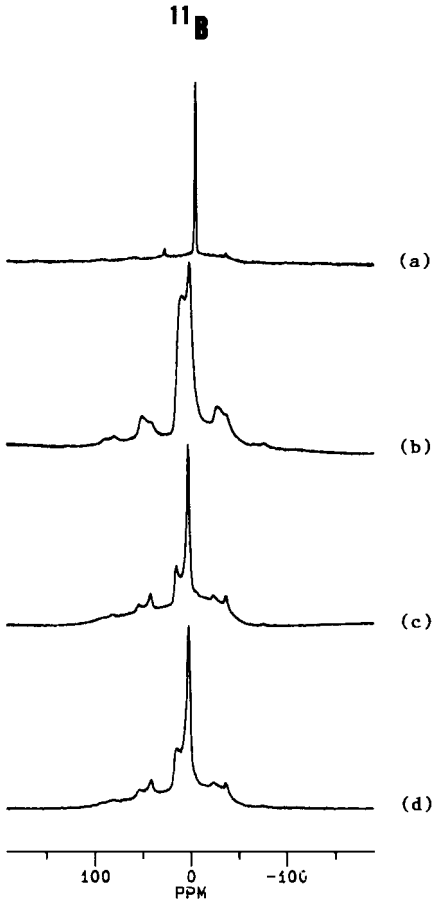

FIG. 6. ^{11}B characteristic MAS NMR spectra of (a) BPO_4, (b) B_2O_3, (c) $Li_2B_4O_7$ and (d) $Na_2B_4O_7$ at 9.4 T (128.38 MHz; 5.6 kHz MAS) ppm from $BF_3 \cdot Et_2O$.

Typical ^{11}B MAS NMR spectra at 11.7 T of APB- and AlB- systems appeared in Figs. 5 and 7, respectively. As boron ions are introduced into the $AlPO_4$ or Al_2O_3 network, a narrow response typical of the four-coordinated boron appear in the ^{11}B spectrum of the APB and AlB systems. So, APB and AlB samples exhibited boron atoms in symmetric four-coordinated tetrahedral sites (BO_4 units), characterized by their highly symmetric Gaussian

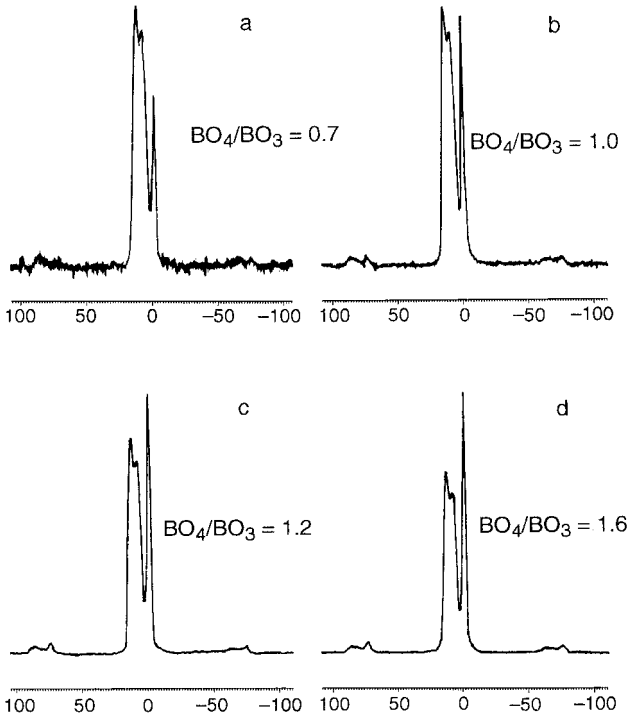

FIG. 7. ^{11}B MAS NMR spectra (11.7 T; 12 kHz MAS): (a) AlB-5-M-573; (b) AlB-9-M-573; (c) AlB-20-M-573; (d) AlB-30-M-573.

shape peak at c.a. −1.4 ppm, and boron atoms in three-coordinated trigonal sites (BO_3 units) exhibiting a doublet at 7−12 ppm range, due to its high quadrupolar interaction.

Moreover, the ^{1}H-^{11}B CP MAS NMR spectra (not shown) reveal that only the boron responsible for the line at c.a. 1.4 ppm (boron in tetrahedral environment) cross-polarizes, confirming that these borons are attached to hydroxyl groups. This is in agreement with the DRIFT results (see below).

It is remarkable that the two coordinations of boron exist on APB- and AlB- systems and, besides, the tetrahedral boron increases with boria loading. Thus, the intensity of the peak at c.a. −1.4 ppm increased with an increase in boron content (see Fig. 7). So, the ratio of BO_4 to BO_3 species increased as boron loading increased (see DRIFT results).

DRIFT Measurements

Several series of DRIFT experiments were completed to understand the effects of boron on $AlPO_4$ and Al_2O_3 supports. The influence of boron on the support was studied by examining the hydroxyl and borate stretching regions. The spectrum of pure amorphous $AlPO_4$, in the OH stretching vibration region (4000–2500 cm^{-1}), recorded after thermal pretreatment at 573 K for 1 h under a nitrogen flow (10 ml min^{-1}), is shown in Fig. 8A (a). Two isolated hydroxyl peaks were found: a weak one at 3785 cm^{-1} and a strong one at 3669 cm^{-1}, which are due to aluminum (with aluminum atoms in tetrahedral coordination) and phosphorus surface hydroxyl groups, respectively (1, 62, 63). Also a very broad band around 3580 cm^{-1} is found. This band is due to surface hydroxyl groups, most likely phosphorus ones, perturbed by a hydrogen bridge bond from a surface hydroxyl band.

The DRIFT spectra of the hydroxyl region of boron modified $AlPO_4$ (APB-M; 5–30 wt% B_2O_3) samples are shown in Fig. 8A (b–e). The incorporation of boron results in the appearance of a new band at about 3696 cm^{-1}, whose intensity increases with boron loading. This frequency compares well with the ν_{OH} of free BOH groups such as those of H_3BO_3 in N_2 cryogenic matrices (64) or on the surface of silica impregnated by boria (65) as well as in amorphous alumina-boria (35) or borate promoted Ni–Mo/Al_2O_3 hydrotreating catalysts (38). So, this band can be assigned to tetrahedral B–OH groups (see ^{11}B CP-MAS NMR results).

Simultaneously with the appearance of the B–OH band, the 3785 and 3669 cm^{-1} OH bands (Al–OH and P–OH, respectively) decrease in intensity. This is more evident when

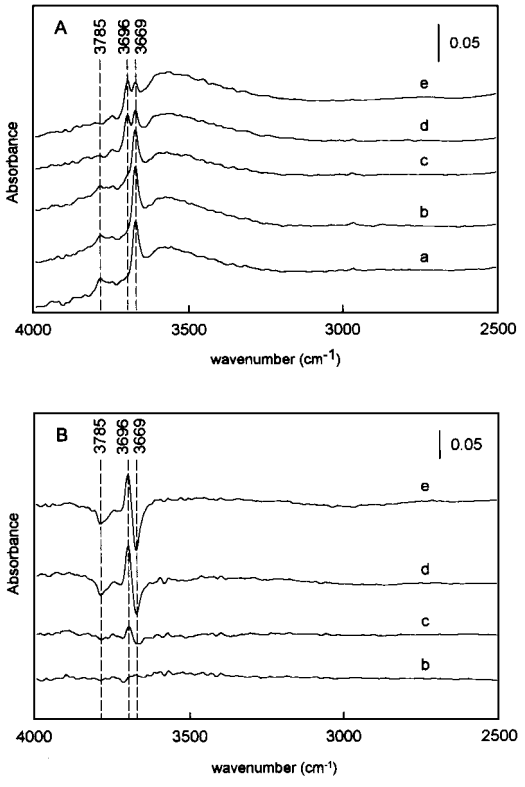

FIG. 8. DRIFT spectra in the hydroxyl region (4000–2500 cm^{-1}) of $AlPO_4$–B_2O_3 samples. (A) Spectra of APB-M catalysts (15 wt% in KBr) rationed automatically against KBr. (B) DRIFT spectra showing negative peaks due to Al–OH and P–OH removal on boria incorporation to $AlPO_4$ (spectrum recorded at 573 K in the nitrogen stream). Reflectance spectra of APB-M samples were ratioed automatically against the pure $AlPO_4$ background (AP-0-M-573). (a) AP-0-M-573; (b) APB-5-M-573; (c) APB-9-M-573; (d) APB-20-M-573; (e) APB-30-M-573. All spectra were displaced for presentation.

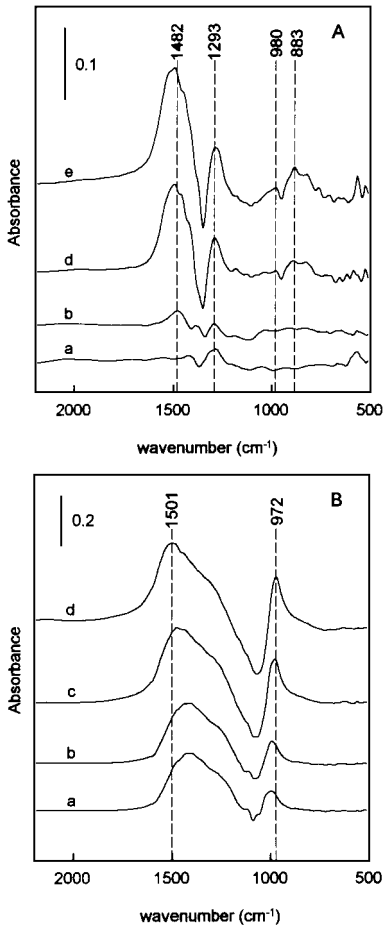

FIG. 9. DRIFT spectra in the skeletal region (2500–500 cm^{-1}) recorded at 573 K in the nitrogen stream. (A) $AlPO_4$–B_2O_3 samples: (a) APB-5-M-573; (b) APB-9-M-573; (c) APB-20-M-573; (d) APB-30-M-573. (B) Al_2O_3–B_2O_3 samples: (a) AlB-5-M-573; (b) AlB-9-M-573; (c) AlB-20-M-573; (d) AlB-30-M-573. Each APB (or AlB) spectrum was rationed automatically against the pure AP (or Al) support background. All spectra were displaced for presentation.

the spectra of each APB sample is ratioed automatically against the pure $AlPO_4$ support (Fig. 8B). Downward bands in these DRIFT spectra are due to the fact that the reference spectra (AP-0-M-573) has more Al–OH and P–OH population than the APB-M catalyst. From Fig. 8B it is evident that as boron loading increases Al–OH and P–OH stretching vibration bands increase downwards in intensity. Notwithstanding, some of the P–OH groups are still present at 30 wt% B_2O_3. Moreover, Al–OH groups almost disappear.

As regards the Al_2O_3 support (results not shown), the incorporation of boron also results in the appearance of boron surface hydroxyl groups (new borate OH groups) showing a DRIFT band at 3689 cm^{-1}. The intensity of this band increases as boron loading increases, as in the case of APB samples. At the same time, the addition of boron results in the disappearance (negative) of a DRIFT band at around 3725 cm^{-1} that is assigned to the basic hydroxy group in Al_2O_3 (38, 66, 67). A DRIFT band at 3666 cm^{-1} is also slightly diminished; this band is assigned to acidic hydroxyl groups in Al_2O_3 (38, 66, 67).

The DRIFT spectra in the skeletal region (2500–500 cm^{-1}) of APB-M and AlB-M (5–30 wt% B_2O_3) samples are shown in Figs. 9A and B, respectively. The spectra showed in Fig. 9 are those obtained for each APB-M (or AlB-M) sample rationed automatically against the pure APB-0-M (or AlB-0-M) background. From DRIFT spectra below 2500 cm^{-1}, a number of bands become evident. Thus, Fig. 9A revealed that as increasing amounts of boron are incorporated, DRIFT bands in the region 1450–1100 cm^{-1} gain intensity. Besides we can observe a small DRIFT band at around 980 cm^{-1}. These bands can be ascribed to the B–O stretches of a borate phase.

In this sense, in boron-oxygen compounds, broad adsorption bands in the region 1500–1200 cm^{-1} are assigned to the asymmetric B–O bond stretching vibrations of trigonal six-membered boroxol rings (BO_3 with bridging oxygen) and non-ring BO_3 units (68–70). These species can also be responsible for an in-plane and an out-of-plane bending band near 740 and 650 cm^{-1}, respectively. In the case of boria, whose spectrum is reported in Fig. 10a, an absorption due to asymmetric B–O stretches extends from 1240 cm^{-1} (main maximum) to 1490 cm^{-1} (69).

Tetrahedral borate species are instead characterized by complex absorptions, in the region 1100–900 cm^{-1}, due to asymmetrical and symmetrical B–O stretching of tetrahedral BO_4 groups (70–72) as in $Li_2B_4O_7$ (Fig. 10c).

The spectra of our APB and AlB samples show that in these materials both trigonal and tetrahedral boron exist on their surface. Moreover, trigonal planar borate species,

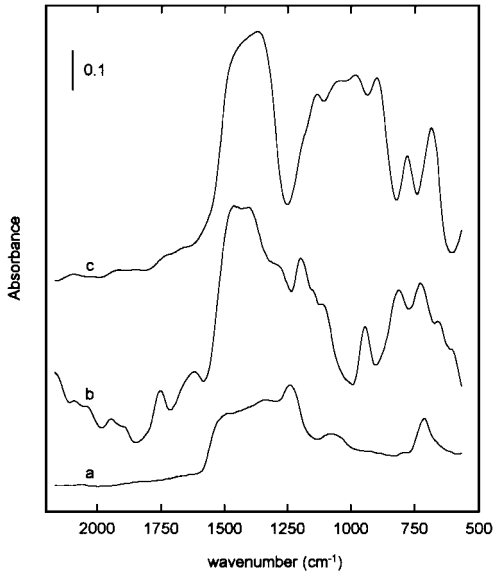

FIG. 10. DRIFT spectra of model boron compounds (15 wt% in KBr): (a) B_2O_3; (b) H_3BO_3; (c) $Li_2B_4O_7$.

responsible for the pair of bands at around 1480 and 1290 cm^{-1} in APB samples, and for a broad band 1500–1100 cm^{-1} (deconvoluted into two bands at around 1470 and 1290 cm^{-1}) in AlB samples, are definitely predominant. However, tetrahedral borate species (band around 980 cm^{-1}) increase with boria loading. These data are in agreement with those found in ^{11}B NMR (see above).

Furthermore, neither B_2O_3 nor its hydration product H_3BO_3, whose spectra appeared in Figs. 10a and 10b, are present in AlB systems as separate phases since the DRIFT spectra in Fig. 9 are different from those in 10a and 10b. So, the DRIFT spectra of the APB and AlB systems is indicative of the presence in their amorphous network of BO_3 (ring and non-ring units) and BO_4 groups. These groups are constituent or larger borate groups, such as diborate, triborate or triborate with one non-bridging oxygen, as exist in the borate glass network (69–74).

Textural Properties

Full nitrogen adsorption–desorption isotherms (77 K) were obtained for all APB and AlB samples after calcination at 473–623 K for 3 h (i.e. for the amorphous APB and AlB samples). The isotherms were akin to type IV of the BDDT classification (75) and the hysteresis loops correspond to type H1 of the classification proposed by the IUPAC (76). These facts strongly suggest that the materials were mesoporous solids. The absence of microporosity, suggested by the shape of the isotherms, was confirmed using the Harkins-Jura correlation (77). Plots of multilayer thickness "t" vs volume of adsorbed nitrogen (V_p) could be extrapolated through the origin. The observed increasing slope of this t-plot in the high-t region also supports the above assignment of pore shape (78).

The specific (BET) surface areas and pore volumes of the APB and AlB systems treated at temperatures in the range 473–623 K are compiled in Table 2, together with the mean pore radii.

The porous texture of the APB and AlB samples was analyzed following the BJH method and assuming a cylindrical pore model (42). The analysis was applied to the adsorption branch of each isotherm, which is to be preferred to the desorption branch for type IV isotherms (78, 79).

APB systems. As shown in Table 2, strong differences are apparent in the textural parameters of the unmodified $AlPO_4$ depending on the solvent of treatment. When methanol is used as solvent, the surface area remained almost unchanged but if water is used as the solvent, the surface area strongly decreased. Pore analysis indicated that this decrease in surface area was accompanied by a decrease in V_p and an increase in the pore size (r_p). Also, the pore size distribution is slightly displaced towards larger pores.

Moreover, Table 2 also shows that the incorporation of boria into $AlPO_4$, develops a slight decrease in surface area and pore volume as boria loading increases. Notwithstanding, the decrease in progressive surface area and pore volume versus boron loading becomes greater (larger) as the boron content of the APB system increases. Furthermore, only at 20–30 wt% B_2O_3 did we observe an increase in main pore radii.

TABLE 2

Textural Properties of the $AlPO_4$–B_2O_3 and Al_2O_3–B_2O_3 Systems[a]

System	$S_{BET}/(m^2\ g^{-1})$	$V_p/(mL\ g^{-1})$	$r_p/(nm)$
AP-773	146	1.29	17.7
AP-0-473	65	0.63	19.3
AP-0-573	62	0.74	23.8
AP-0-623	67	0.63	18.8
APB-9-473	67	0.73	21.8
APB-9-573	66	0.74	22.3
APB-9-623	61	0.81	26.8
AP-0-M-573	143	1.30	18.1
APB-5-M-573	142	1.24	17.4
APB-9-M-573	140	1.22	17.4
APB-20-M-573	131	1.21	18.4
APB-30-M-573	119	1.15	19.3
Al-923	165	0.29	3.5
Al-0-473	223	0.33	2.9
Al-0-573	197	0.31	3.1
Al-0-623	228	0.35	3.1
AlB-9-473	134	0.22	3.3
AlB-9-573	143	0.24	3.4
AlB-9-623	153	0.25	3.2
AlB-0-M-573	165	0.30	3.7
AlB-5-M-573	147	0.27	3.7
AlB-9-M-573	143	0.27	3.7
AlB-20-M-573	124	0.23	3.7
AlB-30-M-573	119	0.22	3.7

[a] From the adsorption branch of the isotherm using the BJH method and cylindrical idealization.

AlB systems. As regards the Al_2O_3 support, the nature of the impregnation solvent substantially affects its textural parameters (Table 2) and, thus, when methanol is used as the solvent, the surface area and pore volume remained almost unchanged, as in the case of $AlPO_4$. When water is used as solvent, surface area and pore volume increase. Furthermore, the increase in thermal treatment (473–623 K) previous boron incorporation modifies the textural parameters slightly.

On the other hand, irrespective of the impregnation medium, the incorporation of boron decreases surface area and pore volume. Besides, this decrease becomes greater as the boron content of the AlB system increases, as in the case of APB systems. Notwithstanding, on the APB systems we observed less of a decrease in the surface area with boron loading as compared to AlB systems.

CONCLUSIONS

Structural and textural characterization of $AlPO_4$–B_2O_3 and Al_2O_3–B_2O_3 systems (5–30 wt% B_2O_3) provides

consistent information about the important changes taking place in $AlPO_4$ and Al_2O_3 surface properties after the incorporation of boron. Thus, we can conclude that:

(1) APB systems remained amorphous after calcination up to 900 K. Moreover, in AlB systems, alumina remained in a γ-Al_2O_3 phase with a low degree of crystallinity after thermal treatment up to 1150 K. Furthermore, in both APB and AlB systems, the crystallization process of the initially amorphous $AlPO_4$ or γ-Al_2O_3 was favoured by the incorporation of boron, and thus α-cristobalite $AlPO_4$ in APB systems and aluminum borate in AlB systems were found.

(2) EDX and XPS indicated a surface enrichment in boron for APB systems while, for AlB ones, the reverse is true.

(3) APB systems with an amorphous structure (i.e. those calcined below 900 K) had only tetrahedral Al in $Al(PO)_4$ environments and P atoms in tetrahedral coordination. Moreover, ^{27}Al MAS NMR showed both tetra and octahedral aluminum in AlB systems. Furthermore, ^{11}B MAS NMR identified both tetrahedral (BO_4) and trigonal (BO_3) species; the former were found to increase with boria loading.

(4) DRIFT spectroscopy showed the presence of B–OH groups and B–O stretches of a borate phase exhibiting both trigonal and tetrahedral boron, strengthening ^{11}B MAS NMR results.

(5) As a consequence less thermal stability in APB and AlB systems compared to $AlPO_4$ and γ-Al_2O_3 supports, a progressive decrease in both surface area and pore volume was found as boron content increases.

ACKNOWLEDGMENTS

The authors acknowledge subsidies from the DGICYT (Project PB92/0816), Ministerio de Educacion y Cultura, and from the Consejeria de Educación y Ciencia (Junta de Andalucia), España. The authors thank Dr. R. Ruiz (NMR Service, Universidad de Cordoba) and Bruker (France) for performing MAS NMR measurements. They also thank Prof. M. Sullivan for linguistic revision of the manuscript.

REFERENCES

1. Bautista, F. M., Campelo, J. M., Garcia, A., Luna, D., Marinas, J. M., and Romero, A. A., *Appl. Catal. A* **96**, 175 (1993), and references cited therein.
2. Campelo, J. M., Garcia, A., Luna, D., and Marinas, J. M., *J. Catal.* **111**, 106 (1988).
3. Campelo, J. M., Garcia, A., Luna, D., and Marinas, J. M., *React. Kinet. Catal. Lett.* **30**, 165 (1986).
4. Campelo, J. M., Garcia, A., Luna, D., and Marinas, J. M., *J. Catal.* **102**, 299 (1986).
5. Campelo, J. M., Garcia, A., Luna, D., and Marinas, J. M., *in* "Preparation of Catalysts IV" (B. Delmon, P. Grange, P. A. Jacobs, and G. Poncelet, Eds.), *Stud. Surf. Sci. Catal.* **31**, 199 (1987).
6. Cativiela, C., Fraile, J. M., Garcia, J. I., Mayoral, J. A., Campelo, J. M., Luna, D., and Marinas, J. M., *Tetrahedron Asymm.* **4**, 2507 (1993).
7. Campelo, J. M., Garcia, A., Herencia, J. F., Luna, D., Marinas, J. M., and Romero, A. A., *J. Catal.* **151**, 307 (1995).
8. Bautista, F. M., and Delmon, D., *Appl. Catal. A* **130**, 47 (1995).
9. Afxantidis, J., Bouchry, N., and Aune, J. P., *J. Mol. Catal. A* **102**, 49 (1995).
10. Campelo, J. M., Garcia, A., Lafont, F., Luna, D., and Marinas, J. M., *Syn. Commun.* **22**, 2335 (1992).
11. Bautista, F. M., Campelo, J. M., Garcia, A., Leon, J., Luna, D., and Marinas, J. M., *J. Chem. Soc., Perkin Trans. 2*, 815 (1995).
12. Blanco, A., Campelo, J. M., Garcia, A., Luna, D., Marinas, J. M., and Romero, A. A., *J. Catal.* **137**, 51 (1992).
13. Bautista, F. M., Campelo, J. M., Garcia, A., Luna, D., Marinas, J. M., and Romero, A. A., *Appl. Catal. A* **104**, 109 (1993).
14. Bautista, F. M., Campelo, J. M., Garcia, A., Luna, D., Marinas, J. M., Romero, A. A., Navio, J. A., and Macias, M., *J. Catal.* **145**, 107 (1994).
15. Campelo, J. M., Garcia, A., Luna, D., Marinas, J. M., Romero, A. A., Navio, J. A., and Macias, M., *J. Chem. Soc., Faraday Trans.* **90**, 2265 (1994).
16. Lindblad, T., Rebenstorf, B., Yan, Z. G., and Andersson, S. L. T., *Appl. Catal. A* **112**, 87 (1994).
17. Andersson, S. L. T., *Appl. Catal. A* **112**, 209 (1994).
18. Kuo, P. S., and Yang, B. L., *J. Catal.* **117**, 301 (1989).
19. Lakshmi, L. J., and Rao, P. K., *Catal. Lett.* **21**, 345 (1993).
20. Lakshmi, L. J., and Rao, P. K., Mastikhin, V. M., and Nosov, A. V., *J. Phys. Chem.* **97**, 11373 (1993).
21. Lakshmi, L. J., Srinivas, S. T., Rao, P. K., Nosov, A. V., Lapina, O. B., and Mastikhin, V. M., *Solid State Nucl. Magn. Reson.* **4**, 59 (1995).
22. Campelo, J. M., Climent, M. S., and Marinas, J. M., *React. Kinet. Catal. Lett.* **47**, 7 (1992).
23. Campelo, J. M., Chakraborty, R., and Marinas, J. M., *Syn. Commum.* **26**, 415 (1996).
24. Campelo, J. M., Chakraborty, R., and Marinas, J. M., *Syn. Commum.* **26**, 1639 (1996).
25. Izumi, Y., and Shiba, Ti., *Bull. Chem. Soc. Jpn.* **37**, 1797 (1964).
26. Sakurai, H., Sato, S., Urabe, K., and Izumi, Y., *Chem. Lett.* 1783 (1985).
27. Sato, S., Kuroki, M., Sodesawa, T., Nozaki, F., and Maciel, G. E., *J. Mol. Catal. A* **104**, 171 (1995).
28. Sato, S., Hasebe, S., Sakurai, H., Urabe, K., and Izumi, Y., *Appl. Catal.* **29**, 107 (1987).
29. Curtin, T., McMonagle, J. B., and Hodnett, B. K., *Appl. Catal. A* **93**, 91 (1992).
30. Curtin, T., McMonagle, J. B., Ruwet, M., and Hodnett, B. K., *J. Catal.* **142**, 172 (1993).
31. Peil, K. P., Galya, L. G., and Marcelin, G., *in* "9th Internat. Congr. Catal.," p. 1712. Calgary, Canada, 1988.
32. Peil, K. P., Galya, L. G., and Marcelin, G., *J. Catal.* **115**, 441 (1989).
33. Wang, W. J., and Chen, Y. W., *Catal. Lett.* **10**, 297 (1991).
34. Li, C., and Chen, Y. W., *Catal. Lett.* **19**, 99 (1993).
35. Delmastro, A., Gozzelino, G., Mazza, D., Vallino, M., Busca, G., and Lorenzelli, V., *J. Chem. Soc., Faraday Trans.* **88**, 2065 (1992).
36. Colorio, G., Vedrine, J. C., Auroux, A., and Bonnetot, B., *Appl. Catal. A* **137**, 55 (1996).
37. Tsai, M. E., Chen, Y. W., Kang, B. C., Wu, J. C., and Leu, L. J., *Ind. Eng. Chem. Res.* **30**, 1801 (1991).
38. DeCanio, E. C., and Weissman, J. G., *Colloids Surf. A* **105**, 123 (1995).
39. Colorio, G., Auroux, A., and Bonnetot, B., *J. Termal Anal.* **38**, 2565 (1992).
40. Colorio, G., Auroux, A., and Bonnetot, B., *J. Thermal Anal.* **40**, 1267 (1993).
41. Simon, S., van der Pol, A., Reijerse, E. J., Kentgens, A. P. M., van Moorsel, G. J., and de Boer, E., *J. Chem. Soc., Faraday Trans.* **90**, 2663 (1994).
42. Barrett, E. P., Joyner, L. S., and Halenda, P. P., *J. Am. Chem. Soc.* **73**, 373 (1951).

43. Yamaguchi, O., Tada, M., Takeoka, K., and Shimizu, K., *Bull. Chem. Soc. Jpn.* **52**, 2153 (1979).
44. Gielisse, P. J. M., and Foster, W. R., *Nature* **195**, 69 (1962).
45. Garsche, M., Tillmanns, E., Almen, H., Schneider, H., and Kupcik, V., *Eur. J. Mineral.* **3**, 793 (1991).
46. Wells, A. F., *in* "Structural Inorganic Chemistry," 5th ed., p. 1065. Clarendon Press, Oxford, 1984.
47. Meera, B., and Ramakhrishna, J., *J. Non-Cryst. Solids* **159**, 1 (1993).
48. Sanz, J., Campelo, J. M., and Marinas, J. M., *J. Catal.* **130**, 642 (1991).
49. Cheung, T. T. P., Willcox, K. W., McDaniel, M. P., Johnson, M. M., Bronnimann, C., and Frye, J., *J. Catal.* **102**, 10 (1986).
50. Muller, D., Jahn, E., Ladwig, G., and Haubenreisser, U., *Chem. Phys. Lett.* **109**, 332 (1984).
51. Blackwell, C. S., and Paton, R. L., *J. Phys. Chem.* **88**, 6135 (1984).
52. Massiot, D., Khan-Harari, A., Michel, D., Muller, D., and Taulelle, F., *Magn. Reson. Chem.* **28**, 582 (1990).
53. Alemany, L. B., and Kirker, G. W., *J. Am. Chem. Soc.* **108**, 6158 (1986).
54. Newnham, R. E., and de Haan, Y. M., *Z. Krist.* **117**, 235 (1962).
55. Fyfe, C. A., Gobbi, G. C., Hartman, J. S., Lenkinski, R. E., O'Brien, J. H., Beange, E. R., and Smith, M. A. R., *J. Magn. Reson.* **47**, 168 (1982).
56. Turner, G. L., Smith, K. A., Kirkpatrick, R. J., and Oldfield, E., *J. Magn. Reson.* **67**, 544 (1986).
57. Engelhard, G., and Michel, D., *in* "High-Resolution Solid-State NMR of Silicates and Zeolites," p. 332. Wiley, New York, 1987.
58. Scholle, K. F. M. G. J., and Veeman, W. S., *Zeolites* **5**, 118 (1985).
59. Bray, P. J., *J. Non-Cryst. Solids* **95/96**, 45 (1987).
60. Simon, S., van Moorsel, G. J. M. P., Kentjens, A. P. M., and de Boer, E., *Solid State Nucl. Magn. Reson.* **5**, 163 (1995).
61. Lai, K. C., and Petch, H. E., *J. Chem. Phys.* **43**, 178 (1965).
62. van Wazer, J. R., *in* "Phosphorus and its Compounds." Vol. 1. Interscience, New York, 1958.
63. Farmer, V. C., *in* "The Infrared Spectra of Minerals." Butterwoths, London, 1974.
64. Ogden, J. S., and Young, N. A., *J. Chem. Soc., Dalton Trans.* 1645 (1988).
65. Morterra, C., and Low, M. J. D., *J. Phys. Chem.* **74**, 1297 (1970).
66. DeCanio, E. C., Edwards, J. C., Scalzo, T. R., Storm, D. A., and Bruno, J. W., *J. Catal.* **132**, 498 (1991).
67. DeCanio, E. C., and Storm, D. A., *J. Catal.* **132**, 375 (1991).
68. Laperches, J. P., and Tarte, P., *Spectrochim Acta.* **22**, 1201 (1966).
69. Broadhead, P., Newman, G. D., *Spectrochim Acta. A* **28**, 1915 (1972).
70. Socrates, G., *in* "Infrared Characteristic Group Frequencies." Wiley, New York, 1980.
71. Ross, S. D., *Spectrochim Acta. A* **28**, 1555 (1972).
72. Denning, J. H., and Ross, S. D., *Spectrochim Acta. A* **28**, 1775 (1972).
73. Krogh-Moe, J., *Phys. Chem. Glasses* **6**, 46 (1965).
74. Konijnendijk, W. L., *Philips Res. Rep. Suppl.* **1**, 1 (1975).
75. Brunauer, S., Deming, L. S., Deming, W. S., and Teller, E., *J. Am. Chem. Soc.* **62**, 1723 (1940).
76. Sing, K. S. W., Everett, D. H., Haul, R. A. W., Moscou, L., Pierotti, R. A., Rouquerol, J., and Siemieniewska, T., *Pure Appl. Chem.* **57**, 603 (1985).
77. Harkins, W. D., and Jura, G., *J. Chem. Phys.* **11**, 431 (1943).
78. Broekhoff, J. C. P., and Linsen, B. G., *in* "Physical and Chemical Aspects of Adsorbents and Catalysts" (B. G. Linsen, Ed.), pp. 1–62. Academic Press, London, 1970.
79. Mata Arjona, A., Parra Soto, J. B., and Otero Arean, C., *Stud. Surf. Sci. Catal.* **10**, 175 (1982).